Investigation of density of states and electrical properties of chemically synthesized Ba$_{0.5}$Co$_{0.5}$Bi$_2$NbTaO$_9$ nanoceramics

Mrinal Kanti Adak[1], Prasanta Dhak[2, 3*], Atreyee Kundu[4], Debasis Dhak[1*]

[1]*Department of Chemistry, Sidho-Kanho-Birsha University, Purulia 723101, India*
[2]*Centre for Materials Science and Nanotechnology, Department of Chemistry,*
University of Oslo, Blindern, N-0315 Oslo, Norway
[3]*Department of Chemistry, Indian Institute of Technology Kharagpur, Kharagpur 721302, India*
[4]*Department of Biological Sciences, Presidency University, Kolkata 700073, India*

[*]Corresponding author. E-mail: debasisdhak@yahoo.co.in, prasanta.dhak@smn.uio.no

ABSTRACT

In this present work, nanocrystalline Co^{2+} and Ta^{5+} substituted barium bismuth niobate Ba$_{0.5}$Co$_{0.5}$Bi$_2$NbTaO$_9$ was synthesized by chemical process. Room temperature single phase, tetragonal structure was confirmed using X-ray diffraction (XRD) study. Average crystallite and particle sizes were found to be 33 nm and 40 nm, when analyzed through XRD and transmission electron microscopy (TEM) respectively. Field emission scanning electron microscopy (FESEM) was used for micro-structural investigation of samples sintered at 950˚C for 4h. The investigation revealed that the material was exhibiting high dielectric constant value of 1017 at Curie temperature (T$_c$), 500˚C when measured at 10 kHz. Impedance spectroscopy analysis showed that above 425˚C, the material exhibited both bulk and grain boundary conductivities which were evidenced from FESEM studies. Density of states, minimum hoping distance, binding energy etc. were studied along with other electrical properties from impedance analysis. Hysteresis behavior was also investigated using polarization study. Copyright © 2016 VBRI Press.

Keywords: Nanomaterials; dielectrics; ferroelectrics; impedance; density of states.

Introduction

Bi-based layered perovskite ferroelectric (BLSF) materials have widely been investigated because of its high Curie temperature (T$_c$), fatigue free, low sintering temperature, and environmentally suitable [1-3]. Chemical formula of this series is expressed as Bi$_2$A$_{m-1}$B$_m$O$_{3m+3}$ = (Bi$_2$O$_2$)$^{2+}$ (A$_{m-1}$B$_m$O$_{3m+1}$)$^{2-}$; A is mono-/ di-/ tri- valent ions or a mixture of them, B is tetra-/ penta-/ hexa-valent ions; m and m^{-1} are numbers of oxygen octahedral and pseudoperovskite units interleaved with the bismuth oxide (Bi$_2$O$_2$)$^{2+}$ layers in the pseudoperovskite layers, respectively [4-6]. This provides an opening to modify a large number of cations at these spots, which essentially can improve the physical properties like ferroelectrics, memory devices, non-linear optical devices, pyroelectric sensors, etc [7-13]. BaBi$_2$Nb$_2$O$_9$ (BBN), SrBi$_2$Nb$_2$O$_9$ (SBN), SrBi$_2$Ta$_2$O$_9$ (SBT) are the most promising candidate of this family because they acquire high spontaneous polarization suitable for information storage applications. However, they experience a serious drawback in regards to high processing temperature and high dielectric loss [14-15].

The investigation of electrical conductivity is very significant for the ferroelectric compounds as many physical properties like dielectric, ferroelectric, and piezoelectric are dependent on the nature and extent of conductivity of the materials. Complex impedance spectroscopy is considered to be a great experimental technique to interface between the electrical and structural properties like dielectric behavior of crystalline as well as amorphous materials [16]. The total dielectric response in polycrystalline material due to various microscopic elements like grain, grain boundary etc. can be resolved by equivalent circuit containing an array of parallel RC elements [17].

Most of the electrical properties are greatly influenced by doping of metal ions or chemical compositions and powder characteristics such as particle size, morphology, purity etc in dielectric materials. There are many reports in open literature aiming to improve the dielectric and ferroelectric properties of BBN by doping different metal ions in suitable sites. [18, 19]. Synthesis procedures are also varied aiming to improve the properties of such materials. The chemical process includes the methods based on co-precipitation [20], hydrothermal synthesis [21], sol-gel technique [19], and aqueous solution based chemical method [22].

Thin films of SrBi$_2$(Ta,Nb)$_2$O$_9$ (SBTN) and Sr$_{0.8}$Bi$_{2.5}$Ta$_{1.2}$Nb$_{0.9}$O$_{9+x}$ were successfully synthesized by Bhattacharyya *et al.* [23] and Tsai *et al.* [24]. Tomar *et al.* [25] have reported preparation of Sr$_{1-x}$Ba$_x$Bi$_2$TaNbO$_9$ and the ferroelectric polarization on Sr$_{0.5}$Ba$_{0.5}$Bi$_2$TaNbO$_9$ film deposited on Pt substrate. Prasad *et al.* [26] have reported Sr$_{1-x}$Ba$_x$Bi$_2$(Nb$_{0.5}$Ta$_{0.5}$)$_2$O$_9$ and Sr$_{0.5}$Ba$_{0.5}$Bi$_2$(Nb$_{1-y}$Ta$_y$)$_2$O$_9$

ceramics prepared by solid state route. La and Nb co-modified $Sr_{0.8}Bi_{2.2}Ta_2O_9$ thin films shown by Haifeng *et al.*, [**27**] who have observed that the remnant polarization was increased from 25 µC/cm^2 to 35 µC/cm^2 for the composition $Sr_{0.8}La_{0.1}Bi_{2.1}(Ta_{0.7}Nb_{0.3})_2O_9$ and $Sr_{0.8}La_{0.1}Bi_{2.1}(Ta_{0.8}Nb_{0.2})_2O_9$ respectively. Recently holmium substituted $SrBi_{2-x}Ho_xTa_2O_9$ (x = 0.00–2.0) compositions [**28**] were synthesized by the solid state technique and the variation of sintering temperature on nanocrystalline $Sr_{0.8}Bi_{2.2}Ta_2O_9$ on the electrical behavior were investigated by Sugandha *et al.* [**29**,**30**]. The frequency depend ac conductivity along with the impedance analysis of $Pb_{1-3x/2}Gd_xTiO_3$ and $Pb_2Bi_3SmTi_5O_{18}$ were reported by Prasad *et al.* [**31**, **32**]. Mekap *et al.* have studied the dielectric and electrical behavior of $ZnSb_2O_4$ ceramics [**33**]. Few reports are available on the electrical characterizations studying the density of states, hopping behavior, binding energy etc along with justified correlations with other observed properties of such ceramic materials [**31**, **32**, **34**].

So the detailed literature review revealed that most of the substituted compounds are studied on SBT or SBN ceramics. There are no reports till date to the best of our understanding on impedance spectroscopy study of Co^{2+} and Ta^{5+} substituted $BaBi_2Nb_2O_9$ respectively at A and B site ions. Therefore, investigation of impedance spectroscopy of $Ba_{0.5}Co_{0.5}Bi_2NbTaO_9$ (abbreviated hereafter as BCBNT) ferroelectric ceramics is of great interest. In this study, we report the synthesis of BCBNT ferroelectric ceramics by chemical route through metal ion based complex precursor decomposition method, material characterization of powder ceramics as well as the sintered ceramics. Ferroelectric, density of states, hopping behavior, binding energy and other electrical properties of the above synthesized material are also reported in this article.

Experimental

Nanocrystalline powders of BCBNT were prepared by chemical process using $Co(NO_3)_2$ 6H$_2$O (Merck, India; 97.00%), $Ba(NO_3)_2$ (Merck, India; 99.99%), $Bi(NO_3)_3$ (Merck, India; 99.99%), Ta_2O_5 (Aldrich, 99.99%), Nb_2O_5 (Aldrich, 99.99%), TEA (triethanolamine) (Merck, India; GR grade), Tartaric acid (Quest Chemicals, Kolkata, India, (99%), NH$_4$OH (25%) (Merck, India, GR grade), and HNO$_3$ (65%) (Merck, India; GR grade).

The stock solutions used were standard solutions of $Ba(NO_3)_2$, $Co(NO_3)_2$ $Bi(NO_3)_3$ and tartarate complex of tantalum and niobium. To synthesize the composition of $Ba_{0.5}Co_{0.5}Bi_2NbTaO_9$, adequate volumes of standard solutions of $Ba(NO_3)_2$, $Co(NO_3)_2$, $Bi(NO_3)_3$, Nb-tartarate and Ta-tartarate complexes were mixed thoroughly in a beaker. The preparation of tantalum-and niobium- tartarate from Nb_2O_5 and Ta_2O_5 respectively were discussed elsewhere [**35**, **36**]. TEA was added three times with respect to the total calculated moles of metal ions taken. The pH of the solution was maintained at 5. The homogeneous precursor solution was then heated on a hot plate at ~ 200°C in controlled heating mode. The details of this technique were discussed by Dhak *et al.* [**37**]. A precursor black fluffy mass was produced at the last stage of its heating on the hot plate. Then the black

precursor mass was calcined at 650 ^{o}C for 2 hr to get the nanocrystalline powder of BCBNT.

The crystal phase of the compound was detected by X-ray diffraction (XRD) (Philips, model: PW 1710) of Bragg angles 2θ (20°≤2θ ≤80°), scanning rate of 2° (2θ) /min and the target, Cu$_{K\alpha}$ (λ = 1.5418 Å). The micro-structural studies were performed through transmission electron microscopy (TEM) (Hitachi H-600) and scanning electron microscopy (SEM) (JEOLJSM 5800). Carbon coated copper grid of 100 mesh was used for sample preparation for TEM analysis. LaB$_6$ filament with operation voltage of 200 kV was used for sample grid examination. For SEM study the calcined powders were made into pellets of diameter 10 mm and thickness ~ 2 mm, using a manual hydraulic press instrument at a pressure of 0.05MPa/cm^2. 5% polyvinyl alcohol (PVA) was added to reduce the brittleness of the pellet, which was decomposed out during sintering. The pellets were sintered at 950°C for 4 h in static air. Electrical properties were studied using a computer operated impedance analyzer (HIOKI LCR bridge, Japan). flat surface of both sides of the pellets were polished after sintering and electroded with high puribnjty silver paint. The painted pellets were then dried at 200 $^\circ$C for 2 h for the removal of adsorbed moisture if any. Polarization was studied using aix ACT Multilayer Test Bench (Germany).
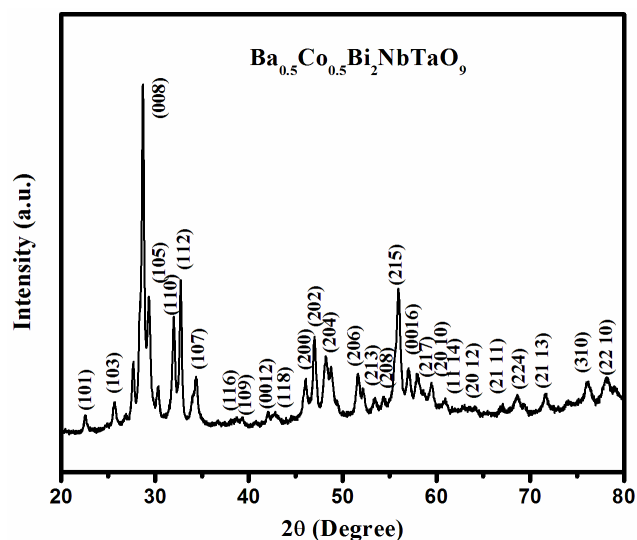
Fig.1. X-ray diffraction study of $Ba_{0.5}Co_{0.5}Bi_2NbTaO_9$ ceramics powder calcined at 650˚C, 2h.

## Results and discussion

Structure and microstructure

The XRD pattern of the sample calcined at 650 ^{o}C for 2 hr is shown in **Fig. 1** at 2θ range from 20° to 80°, scanning speed 2° 2θ/min. The tetragonalsingle-phase structure having space group *I4/mmm* of the compound with no secondary phase was confirmed after analyzing the X-ray data. The average lattice constants along with the single unit cell volume were calculated to be a = 3.9394 Å, c = 24.456 Å, and 397.05 Å^3 respectively. The standard deviations (SD) were estimated to be 0.0010 and 0.0147 for a and c respectively. However, X-ray data for $BaBi_2Nb_2O_9$ and $BaBi_2Ta_2O_9$ were refined by earlier workers in tetragonal space group I4/mmm having prototype cell

a = 3.9364, 3.9355Å and c = 25.6386, 25.5686Å respectively [38, 39]. The crystallite size (D) of the synthesized compound was determined from the broadening of XRD peaks using the Scherrer's equation [40], $D = 0.89\lambda/\beta_{1/2}\cos\theta$, where, $\beta_{1/2}$ = half-peak width and λ = wavelength of the target material used and the average value of D was found to be 38 nm.

Fig. 2(a) represents the bright field TEM for BCBNT powder calcined at 650 °C, 2 hr. The particles having almost-spherical morphology was observed with uniform distribution of particle-size as shown in the **Fig. 2 (b)**, although some particles are over focused as indicated by the black spots and some are under focused as indicated by white spots as shown in **Fig. 2 (a)**. The average particle diameter was observed to be 34 nm when calculated by UTI image tool software (version 3.0); the value was in well proximity with the crystallite size obtained from XRD.

(a)

(b)
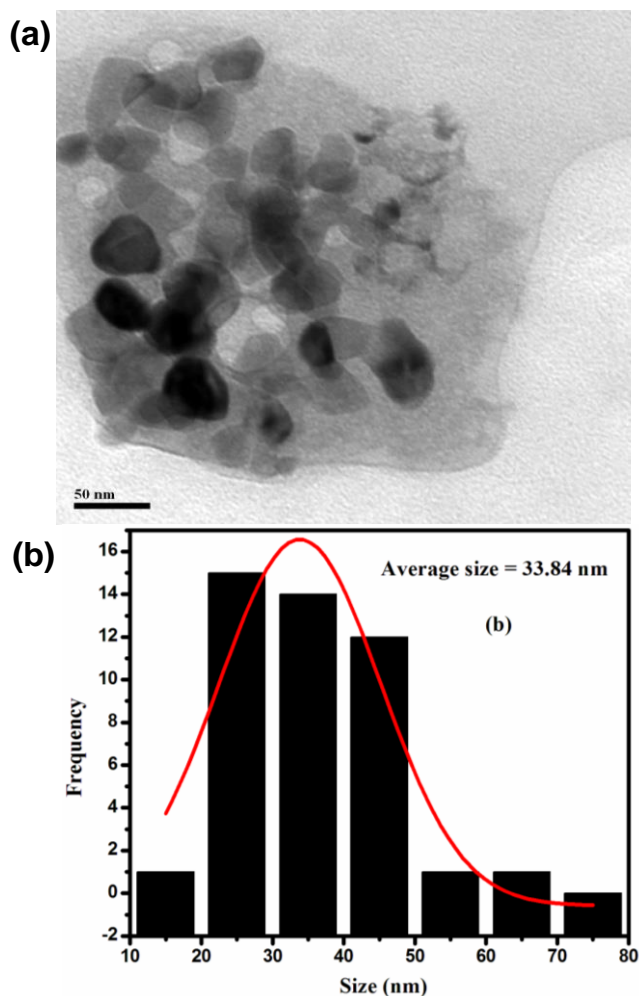
Fig. 2. Transmission electron micrograph of $Ba_{0.5}Co_{0.5}Bi_2NbTaO_9$ ceramics powder calcined at 650 °C for 2h.

The surface property and microstructure as shown in **Fig. 3** was observed from scanning electron micrograph of the surface of the sintered sample at room temperature. Well-developed grains were found with average grain size 0.45μm. ''UTHSCA'' image tool software (version 3) 1995 - 2002, The University of Texas Health Science Center, San Antonia, USA) was used for the estimation of grain size. 96% of the theoretical density was found on sintered pellets while measured using the Archimedes law. Well-defined grains with grain boundaries were clearly observable which was also confirmed from the impedance spectra analysis (discussed later). Adamczyk *et al.* [**41**] also have reported similar type of SEM micrograph earlier.
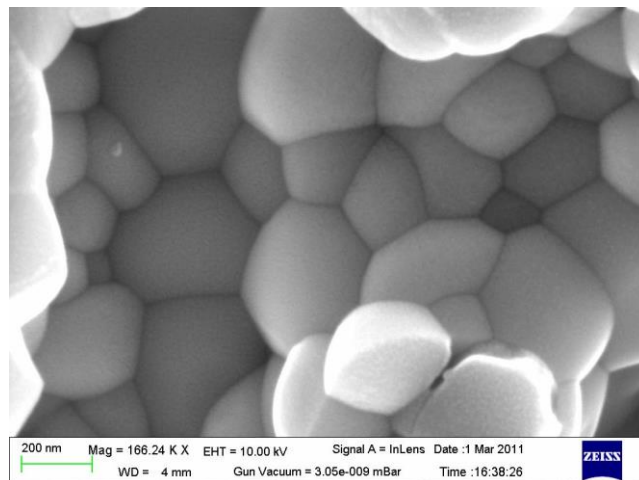
Fig. 3. Field emission scanning electron microscopy of $Ba_{0.5}Co_{0.5}Bi_2NbTaO_9$ ceramic sintered at 950 °C for 4h.

Dielectric studies

The change of dielectric constant (ε') and dielectric loss (tan δ) with temperature at frequencies 1 kHz, 10 kHz, 100 kHz, and 1 MHz are plotted in **Fig. 4 (a)** and **(b)** respectively. ε' vs T (°C) plots indicated the normal ferroelectric behavior, maximum dielectric constant (ε'_{max}) of 1021 at Curie temperature (T_c), 500°C when measured at 10 kHz. The dielectric constant and loss at room temperature were found to be 208 and 0.19 respectively at 10 kHz. There was an increase in dielectric loss with increasing temperature might be due to the higher dc conductivity at increased temperature. The dielectric properties and other general characteristics are summarized in **Table 1**. ε'_{max} of BCBNT was found to be increased from 425 for pure BBN to 1021 for BCBNT whereas the T_cs were found to be increased to 500 °C for BCBNT from 150 °C for pure BBN [**18**] when measured at 10 kHz. The dielectric loss (tan δ) was found to increase to a significant amount from 0.15 for pure BBN [**18**] to 3.48 as listed in **Table 1**.

Table 1. Curie temperature, dielectric constant and loss at different frequencies.

Frequency	Curie temperature (°C)	ε at Curie temperature (°C)	ε at r.t	loss at r.t	loss at Curie temperature
1 kHz	500	2533.2	264.5	0.64	4.99
10 kHz	500	1021.7	197.4	0.20	3.48
100kHz	500	322.1	172.5	0.09	1.73
1 MHz	500	151.6	162.4	0.07	0.69

However $BaBi_2NbTaO_9$ showed high dielectric peak 528 at a Curie temperature of 375 °C [**26**]. Therefore Ni-substituted $BaBi_2NbTaO_9$ increased the

Curie temperature with little decrease of dielectric maxima. This high T_c could be due to the fact that the large size of Ba^{2+} ion ($r_{Ba}^{2+} = 1.61$ Å) was partially replaced by small size Co^{2+} ion ($r_{Co}^{2+} = 0.90$ Å) in BCBNT resulting the change in T_c from 150 °C of pure BBN [18] to 500 °C. Introducing smaller ions into A site and hence occupying less space resulted an enhancement of the rattling space. As a consequence, there was increase in T_c associated with lower ε' with increasing the displacement of cations. As the ionic radii of Nb^{5+} and Ta^{5+} are similar, they do not play significant role on the size effect of Curie temperature in BCBNT ceramics.
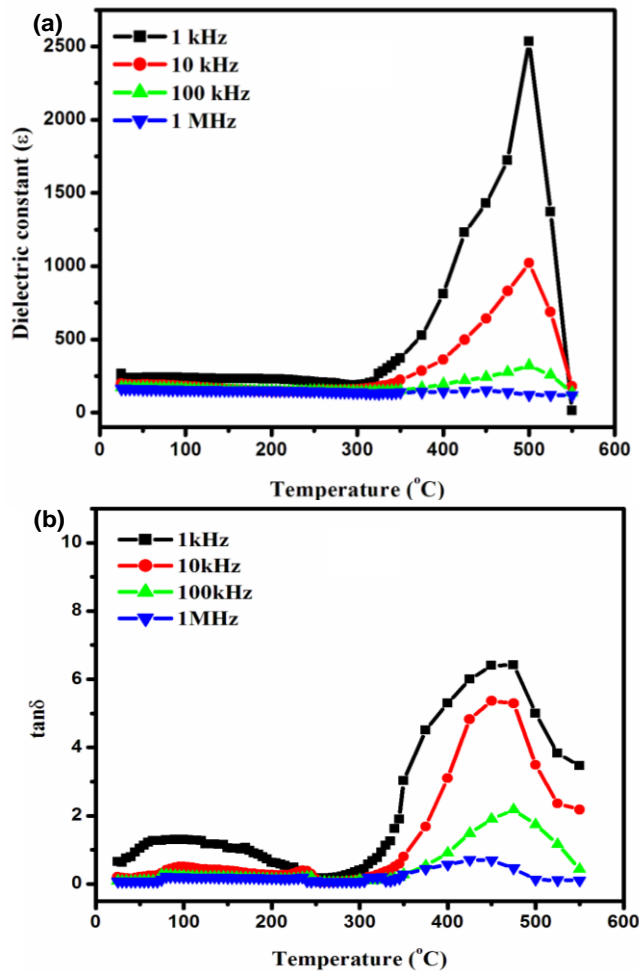
Fig. 4. Temperature variation of (a) dielectric constant and (b) dielectric loss for BCBNT measured at different frequency.

Impedance spectroscopy studies

The electrical properties of $Ba_{0.5}Co_{0.5}Bi_2NbTaO_9$ were investigated using complex impedance spectroscopy. A set of complex impedance spectrum (Nyquist diagram) as shown in **Fig. 5** measured at different temperatures from 370 °C to 525 °C over a wide frequency range (50 Hz–1 MHz). As shown in **Fig. 5 (c)** and **Fig. 5 (d),** the hemispherical arcs appeared at different frequency ranges; one at a higher frequency while another at a lower frequency. The high frequency half circle (first arc) as indicated in **Fig. 5** could be owing to the bulk (grain) property of the material represented by a parallel

combination of bulk resistance (R_b) and bulk capacitance (C_b) of the materials [**42**].

Fig. 5. Complex impedance spectra of BCBNT at different temperatures. The values of capacitance (C_b) were determined from the hemispherical plots, using the relation,

$$((2\pi f)(R_b C_b) = 1 , \tag{1}$$

$$C_b = \frac{1}{2\pi f R_b} , \tag{2}$$

where, R_b and C_b refer to bulk resistance and capacitance respectively; f is the relaxation frequency. This relation is also applicable for grain boundary effects.

Table 2. Variation of electrical parameters (a) bulk (b) grain boundary as a function of temperature.

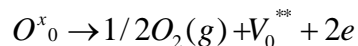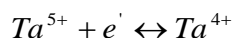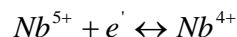| Temperature (°C)	R_b (Ω)	C_b (pF)	$\sigma_{dc\,(b)}$ (s/m)	R_{gb} (Ω)	C_{gb} (pF)	$\sigma_{dc(gb)}$ (s/m)
350	3.35E+05	1.58E+02	5.39E-05	-	-	-
375	9.51E+04	1.12E+02	1.90E-04	-	-	-
400	3.61E+04	1.26E+02	5.00E-04	-	-	-
425	1.61E+04	1.04E+02	1.12E-03	-	-	-
450	8.25E+03	1.29E+02	2.19E-03	1.11E+04	1.43E+03	1.62E-03
475	7.32E+03	1.09E+02	2.47E-03	8.85E+03	1.20E+03	2.04E-03
500	6.33E+03	1.01E+02	2.85E-03	1.18E+04	9.01E+02	1.53E-03
525	7.26E+03	7.31E+01	2.49E-03	2.61E+04	3.05E+02	6.92E-04

b: bulk   gb: grain boundary

The values of capacitance (C_b) determined from the hemispherical plots at different temperatures were calculated to be in the order of pico Farad (pF) as listed in **Table 2**, could be ascribed to the occurrence of grain interior [43]. The capacitance (C_b) in the order of nano Farad (nF) was reported earlier by Misra *et al.*, [44]. Until 425°C as shown in **Fig. 5** (**a**) and (**b**), the material showed only bulk properties and C_bs were found to be 261, 212, 227, and 201 pF respectively at 350, 375, 400 and 425°C. The low frequency curve of impedance spectra were observable at higher temperature from 450°C upto 525°C as shown in **Fig. 5** (**c**) and (**d**). The low frequency half circle (second arc) could be owing to the grain boundary property of the material represented by a parallel combination of grain boundary resistance (R_{gb}) and grain boundary capacitance (C_{gb}) of the materials. The predictable values of both R_b and R_{gb} and their corresponding C_b and C_{gb} at different temperatures are listed in **Table 2**.

The appearance of second semicircular arc at higher temperatures (450°C - 525°C) [**Fig. 5 (c) and Fig. 5 (d)**] exhibited further properties of the material coming up from the grain boundaries (R_{gb}). Hence R_b and R_{gb} effect could be resolved at these temperatures. It could also be noticed that the peak maxima of the plots decreased and the frequency maxima (f_{max}) shifted to the higher end on increasing temperature. As shown in SEM micrograph in **Fig. 3**, the grains were separated by distinct grain boundaries which were in well accordance with the interpretation from the impedance spectrum analysis.

It could be seen that the complex impedance plots were not befitted by full semicircles, rather the hemispherical arcs was dejected and the centre of the hemisphere lies

below the real (Z') axis, which suggested the non-Debye type polydispersive relaxation in BCBNT [45]. The absence of third semicircle suggested a negligible contribution of the electrode-materials interface to impedance.

Fig. 6. Variation of bulk DC conductivity with inverse of temperature for BCBNT.

D.C. conductivity

The variation of bulk conductivity (σ_b) as a function of temperature of the BCBNT compound is shown in **Fig. 6.** Corresponding activation energy using Arrhenius plot of dc conductivity [46] was calculated and was found to be 0.51 eV. The activation energy calculated from σ_b vs 1/T plot (**Fig. 6**) was nearly similar with that of the activation energy estimated from the relaxation time plot (not shown here). The close similarity of the two values indicated the same type of charge carriers for the relaxation and the conduction processes. The value of conductivity at 500 °C is 2.85×10^{-3} S/cm. However the conductivity values did change much in the temperature range from 475°C to 525°C as shown in **Fig. 6**. The variation of grain boundary conductivity with temperature was observed from 450 °C and was found to be 1.62×10^{-3} S/cm. Although the grain boundary conductivity were found to increase from 450°C to 475°C ($\sigma_{gb} = 2.04 \times 10^{-3}$ S/cm) the corresponding values were found to be decreased afterward up to 525°C as listed in **Table 2**.

The value of the activation energy evidently recommended a possibility that the oxygen vacancies might be the charge carriers for conduction in the higher temperature range. Oxygen vacancies are considered as one of the mobile charge carriers in perovskite ferroelectric materials, [47] and ionization of oxygen vacancies creates conduction of electrons mostly in titanates, a process defined as the Kroger-Vink notation [48].

$$O^x_0 \rightarrow 1/2 O_2(g) + V^x_0$$

$$V^x_0 \rightarrow V^* + e'$$

$$V^*_0 \leftrightarrow V_0^{**} + e'$$

Thus oxygen vacancies along with excess electrons are formed in the reduction reaction,

$$O^x_0 \rightarrow 1/2O_2(g) + V_0^{**} + 2e$$

And they may bond to Nb^{5+} and Ta^{5+} in the form,

$$Nb^{5+} + e' \leftrightarrow Nb^{4+}$$

$$Ta^{5+} + e' \leftrightarrow Ta^{4+}$$

These electrons are captured by Nb^{5+} or Ta^{5+} ions or oxygen vacancies are thermally activated, and hence increasing the conduction process. In perovskite ferroelectrics doubly charged oxygen vacancies are considered to be the most mobile charge carriers and play significant role in conduction mechanism [49].
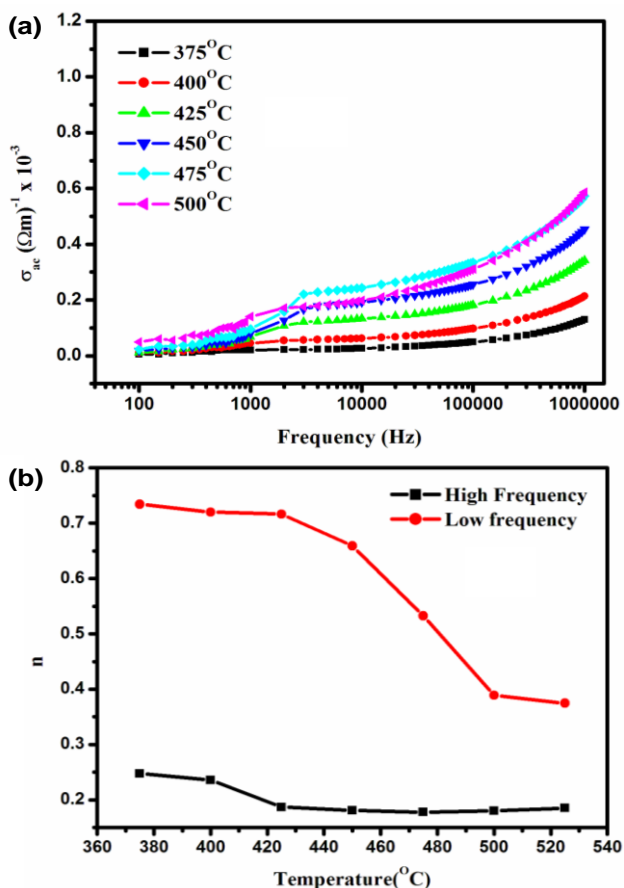
Fig. 7. (a) Variation of AC conductivity with frequency at different temperature (b) Johnscher's frequency exponent (n) at low and high frequency region of BCBNT.

AC conductivity and density of states

As proposed by Jonscher, the frequency dependent conductivity was the originated due to the relaxation of ionic atmosphere after progressing the particle. The variation of AC conductivity with frequency at different temperature is shown in **Fig. 7(a)**. According to Jonscher the ac conductivity can be expressed by the universal power law [50]:

$$\sigma(\omega) = \sigma(0) + \sigma\omega^n \quad (3)$$

where, $\sigma(0)$ is the "dc" or frequency independent part, which is associated to dc conductivity and the next phrase is of constant phase element (CPE) type; n is a frequency exponent in the range of $0 \leq n \leq 1$. The increasing tendency of σ_{ac} might be due to the randomness of cations between the neighboring spots and due to the occurrence of space charges which disappeared at higher frequency and temperature. "Hopping frequency ω_p" which takes place at a particular frequency at the change in slope [51].
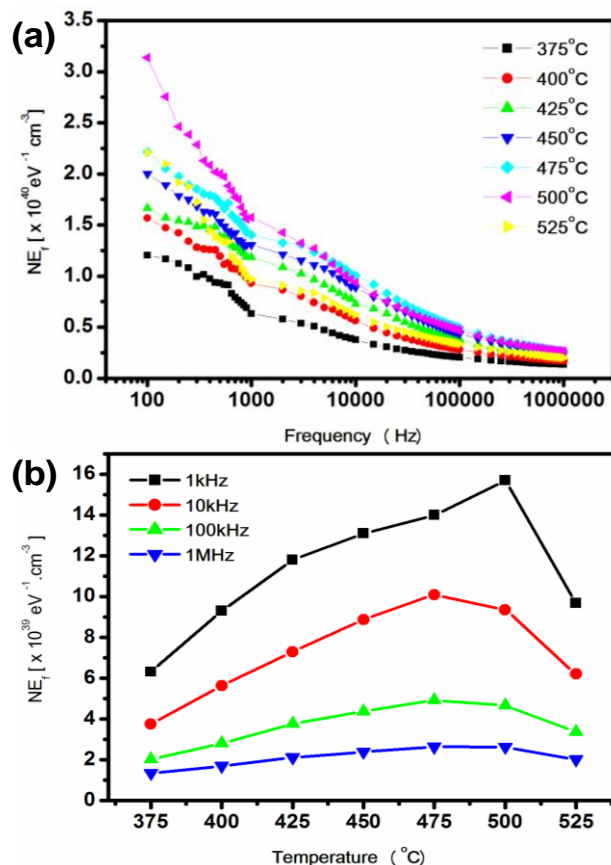
Fig. 8. (a) Dependence of density of states, $N(E_f)$ at Fermi level on frequency at various temperatures and (b) and the temperature dependence of $N(E_f)$ at various frequencies.

Since the frequency exponent, n was dependent on both frequency and temperature, the values of n could be evaluated from the slopes of plots log σ_{ac} vs log ω as shown in **Fig. 7(a)** in the low and high frequency regions at different temperatures as shown in **Fig. 7(b)**. It was observed that n values were decreased with the rise of temperature. At high frequency region (above hoping frequency region [51], n→0 which indicated that the conductivity is almost not dependent on frequency while at lower frequency region the high value of n indicated that the conduction process is dependent both on frequency as well as temperature as observed in **Fig. 7 (b).** Therefore, the conduction process could be regarded as the short range translational type hoping of charge carriers [52, 53]. The mechanism of hopping conduction is usually reliable with the presence of high density of states represented by $N(E_f)$ in any material having a band gap close to a semiconductor. The values of $N(E_f)$ were estimated using formula described by K. Prasad *et al.* [54], at various operating

temperatures as well as frequencies shown in **Fig. 8 (a)** and **Fig. 8 (b)** respectively. It was observed that the $N(E_f)$ values decreased with increasing frequencies and increased with increasing temperature respectively. Therefore, the electrical conduction of the system was influenced by both frequency as well as temperature at low frequency region, while at higher frequency region the charge carriers are thought to be confined and are affected by thermal activation. Reasonably the high $N(E_f)$ values suggested that the hopping between the pairs of spots subjugated by the mechanism of charge transport in BCBNT. However above 475 °C density of states values were observed to follow a decreasing trend which suggests low transport of charge carriers. This observation was also confirmed by low degree of conductivities at this temperature range as observed in **Fig. 7 (a)**. This low density of states values might be due to the high dielectric values in the Curie temperature ($T_c = 500$°C) region as depicted in **Fig. 4 (a)**.
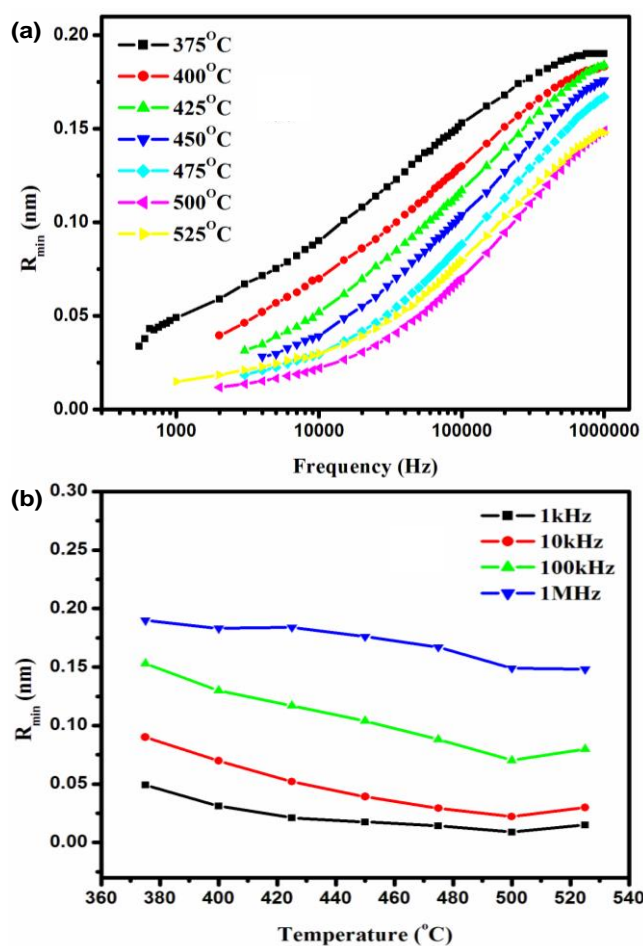
Fig. 9. (a) Dependence of R_{min} of BCBNT on high frequency range at various temperatures and (b) the variation of R_{min} on temperature at various frequencies.

The minimum hopping distance (R_{min}) values were also calculated using the formula,

$$R_{min} = \frac{2e^2}{\Pi \varepsilon \varepsilon_0 W_m} \qquad (4)$$

where, W_m is the binding energy, which is measured as the energy necessary to remove an electron absolutely from one spot to another spot. ε and ε_0 are the dielectric permittivity in the BCBNT and in vacuum respectively. **Fig. 9 (a)** represented as the variation of R_{min} with frequency at various temperatures ranging from 375 °C to 525 °C. The R_{min} values were found to be increased with increasing frequency and also to be increased with increasing temperature. However, there is a minimum value obtained at 500°C compared to the values obtained at 525°C. Interestingly the density of states was also found to quite low as compared to the values obtained at other temperatures as shown in Fig. 9 (a). The R_{min} values were found to be decreasing with increasing temperature as shown in **Fig. 9 (b)** however there is a decreasing trend above 500°C. The R_{min} value at 500°C temperature was found to be 14.9 nm when measured at 1 MHz.

Polarization hysteresis

For any ferroelectric material polarization hysteresis is an important characteristic. **Fig. 10** shows well defined P-E (polarization and applied field) hysteresis loop of BCBNT pellet sintered at 1000°C for 4 h. The measurement experiment was performed at an applied voltage of 6 kV/cm at room temperature. The result of P-E hysteresis measurement elucidated a saturated polarization of $P_s = 0.26$ $\mu C/cm^2$ with a remnant polarization (P_r) of 0.146 $\mu C/cm^2$ and coercive field of 2.6 kV/cm whereas pure BBN sintered at 1000 °C showed coercive field, EC = 9.5 kV/cm and a remnant polarization, $P_r = 1.6$ $\mu C/cm^2$ at an applied voltage of 70 kV/cm [**20**]. These values are consistent with the new generation NVRAMs. It is worthy to mention that the ferroelectric properties found are dependent on density of sintering and defects present in the sample.
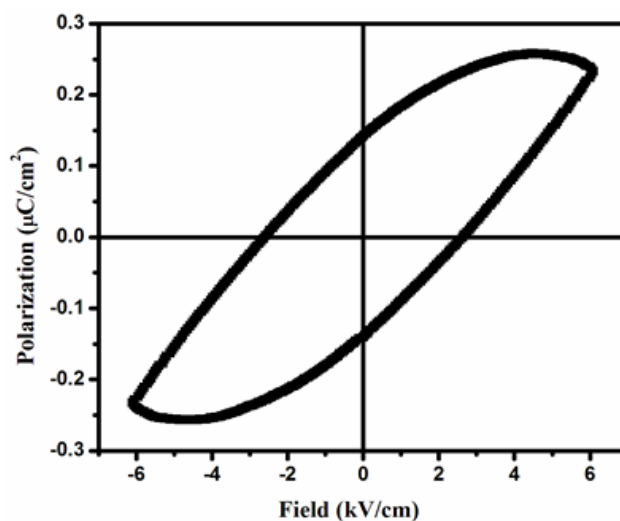
Fig. 10. Hysteresis behavior of BCBNT ceramic pellet sintered at 950°C for 4 h.

Conclusion

Single phase nanocrystalline $Ba_{0.5}Co_{0.5}Bi_2NbTaO_9$ was prepared by a chemical route at a very low temperature of 650°C, 2 hr. The average particle size was calculated to be 33nm with a narrow particle size distribution. 96% relative

density was possible to achieve after sintering the pelleted material just at 950˚C for 4 hr. A very high dielectric constant 1021 was observed at T_c, 500˚C with relatively low dielectric loss. Impedance analysis revealed that, below 425˚C the material exhibited bulk conductivity only while above which it showed both bulk as well as grain boundary conductivity in the order ranging from 10^{-3} to 10^{-5} S/cm. The grain boundary conductivity behavior was also supported by FESEM studies. The activation energy for the DC conductivity was obtained from Arrhenius plot and found to be 0.51 eV which is in good agreement with many earlier reports. Oxygen vacancies were found to be one of the mobile charge carriers; the mechanism was established based on Kroger-Vink notation. At higher frequency region Johnscher frequency exponent, n→0 indicated that the conductivity was almost frequency independent while at lower frequency region the high value of n indicated that the conduction process was dependent both on frequency as well as temperature. The hopping conduction mechanism which was reliable with the presence of high density of states in the order of 10^{49} throughout the frequency and temperature range studied. The minimum hoping distance, R_{min} values were found to be increased with increasing frequency and also to be increased with increasing temperature. The R_{min} value at 500˚C temperature was found to be 14.9 nm when measured at 1 MHz. P-E hysteresis measurement revealed a saturated polarization of P_s = 0.26 μC/cm^2 with a remnant polarization of 0.146 μC/cm^2 and coercive field of 2.6 kV/cm. The detailed electrical characterizations will be helpful for studying other similar type of materials for extensive electronics applications.
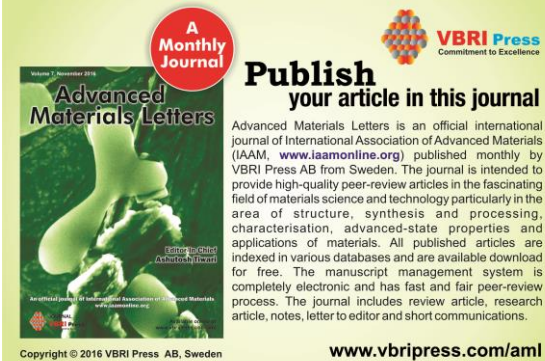
Reference

1. Arauzo, C. A. P.; Scott, J. F.; Ferroelectric Memories, *Science* **1989,** *246*, 1400.
   DOI: 10.1126/science.246.4936.1400
2. Park, B. H.; Kang, B. S.; Bu, S. D.; Noh, T. W.; Lee, J.; Jo, W.; *Nature,* **1999**, *401*, 682.
   DOI: 10.1038/44352
3. Ando, A.; Kimura, M.; Sakabe, Y.; *Jpn. J. Applied Phys.* **2003**, *42*, 2009.
4. Aurivillius, B.; *Arkiv Kemi*. **1994**, *1*, 499.
   ISSN: 0365-6128; English; Accession Number: WOS: A1950XY97600004
5. Aurivillius, B.; *Arkiv Kemi*, **1950**, *2*, 519.
   Accession Number: WOS: A1951XY98200003; **ISSN**: 0365-6128
6. Subbarao, E. C.; *J. Phys. Chem. Solids,* **1962**, *23*, 665.
   DOI: 10.1016/0022-3697(62)90526-7
7. Suman, C. K.; Prasad, K.; Choudhary, R. N. P.; *Phys. Stat. Sol. A,* **2004**, *201A*, 3166.
   DOI: 10.1002/pssa.200406863
8. Qualla, M.; Elaatmani, M.; Daoud, M.; Mezzane, D.; Luk'yanchuk I.; and Zegzouti, A., *Solid State Commun.*, **2004**, *130*, 777.
   DOI: 10.1016/j.ssc.2004.04.017
9. Hornebecq,V.; Elissalde, C.; Porokhonskyy,V.; Bovtun,V.; Petzelt,J.; Gregara, I.; Maglione, M.; Ravez,J.; *J. Phys. Chem. Solids*, **2003**, *64*, 471.
   DOI: 10.1016/S0022-3697(02)00342-6
10. Rao, K. S.; Prasad,T. N. V. K. V.; Subrahmanyam, A. S. V.; Lee, J. H.; . Kim, J. J.; Cho, S. H.; *Mater. Sci. Eng. B,* **2003**, *B98*, 279.
    DOI: 10.1016/S0921-5107(03)00064-3
11. Neurgaonkar, R. R.; Kcory, W.; Ho, W. W.; Hall, W. F.; *Ferroelectrics,* **1981**, *38*, 857.
12. Zheng, X. H.; Chen, X. M.; Zeng, Y. W.; *J. Mater. Sci. Mater. Electron.***2004**, *15*, 733.
13. Bijumon, P. V.; Kohli, V.; Prakash, O.; Verma M. R.; Sabastian, M. T.; *Mater. Sci. Eng. B,* **2004**, *113B*, 13.
    DOI: 10.1016/j.mseb.2004.05.023
14. Scott, J. F.; Thin Film Ferroelectric Materials and Devices, edited by R. Ramesh (Kluwer, Norwell, MA, **1997**, 115.
    DOI: 10.1007/978-1-4615-6185-9
15. Scott, J. F.; *Annu. Rev. Mater. Sci.* 1998, *28*, 79.
    DOI: 10.1146/annurev.matsci.28.1.79
16. Prabhakar, K,; Rao, S. P. M.; *J. Alloys Compd*. **2007**, *437*, 302.
    DOI: 10.1016/j.jallcom.2006.07.108
17. Rout, S. K.; Hussain, A,; Lee, J. S.; Kim, I. W.; Woo, S. I.; *J. Alloys Compd.***2009**, *477*, 706.
    DOI: 10.1016/j.jallcom.2008.10.125
18. Karthik, C. K.; Verma, K. B. R.; *Materials Science and Engineering B*, **2006**, *129*, 245.
    DOI: 10.1016/j.mseb.2006.02.009
19. Kato, K.; Zheng, C.; Finder, J. M.; Dey, S. K.; *Am. Ceram. Soc.***1998**, 81.
    DOI: 10.1111/j.1151-2916.1998.tb02559.x
20. Gaikwada, S. P.; Potdar, H. S.; Violet, S.; Ravi, V.; *Ceram. Int.,* **2005**, *31*, 379.
    DOI: 10.1016/j.ceramint.2004.05.024
21. Muthurajan, H.; Rao, N. K.; Gupta,U. N.; Pradhan, S.; Jha, R. K.; Kumar, H. H.; Mirji, S. A.; Ravi, V.; *Mater. Res. Bull.***2008**, *43*, 1842.
    DOI: 10.1016/j.materresbull.2007.07.006
22. Dhak, P.; Kundu, A.; Pramanik, K.; Pramanik, P.; Dhak, D.; *Adv. Mater. Lett.* **2015**, *6*, 492.
    DOI:10.5185/amlett.2014.5752
23. Bhattacharyya, S.; Bharadwaja, S. S. N.; Krupanidhi, S. B.; *Solid State Communications*. **2000**, *114*, 585.
    DOI: 10.1016/S0038-1098(00)00104-6
24. Tsai, M. S.; Tseng, T. Y.; *Thin Solid Films.* **2000**, *372*, 190.
    DOI: 10.1016/S0040-6090(00)01057-9
25. Tomar, M. S.; Melgarejo, R. E.; Dobal, P. S.; Jain, M.; Katiyar, R. S.; *Journal of Materials Science.***2001**, *36*, 3919.
    DOI: 10.1023/A:1017914020297
26. Shyam Prasad, N.; Verma, K. B. R.; *Materials Research Bulletin* **2003**, *38*, 195.
    DOI: 10.1016/S0025-5408(02)01049-8
27. Shi, H.; Yang, C.; Lin, Y.; Tang, T.; *Integrated Ferroelectrics,* **2006**, *79*, 179.
    DOI: 10.1080/10584580600659472
28. Sugandha, Jha, A. K. ; *Ceramics International.,* **2013**, *39*, 9397.
    DOI: 10.1016/j.ceramint.2013.05.056
29. Sugandha & Jha, A. K. ; *Ferroelectrics.***2014**, *459*, 160.
    DOI: 10.1080/00150193.2013.849518
30. Desu, S. B. ; Li, T. ; *Mat. Sci.& Eng. B.* **1995,** *34*, L4.
    DOI: 10.1016/0921-5107(95)01232-X
31. Parashar, S. K. S.; Chaudhuri, S.; Singh, S. N.; Mahmood, G.; *Applied Physics,***2013**, *7*, 267.
    DOI: 10.1186/2251-7235-7-26
32. Prasad, K.; Suman, C. K.; Choudhary, R. N. P.; *Advances in Applied Ceramics.***2006**, *105*, 258.
    DOI: 10.1179/174367606X115940
33. Mekap, A.; Das, R. P.; Choudary, R. N. P.; *Adv. Mat. Lett.,* **2014**, *5*, 152.
    DOI: 10.5185/amlett.2013.fdm.65
34. Mollah, S.; Som, K. K.; Bose, K.; Choudhuri, B. K.; *J. Applied Physics*, **1993**, *74*, 931.
    DOI: 10.1063/1.355328
35. Dhak, D.; Biswas S. K.; Pramanik, P.; *J. Eur. Ceram. Soc.***2006**, *26*, 3717.
    DOI: 10.1016/j.jeurceramsoc.2005.12.002
36. Dhak, P.; Dhak, D.; Pramanik, P.; *Materials Science: Materials in Electronics,* **2011**, *22*, 1750.
    DOI: 10.1007/s10854-011-0358-1
37. Dhak, D.; Pramanik, P.; *J. Am. Ceram. Soc.,* **2006**, 89, 1014.
    DOI: 10.1111/j.1551-2916.2005.00769.x
38. Ismundar; Kennedy, B. J.; *J. Mater. Chem.***1999**, *9*, 541.
    DOI: 10.1039/A806760K
39. Macquart, R.; Kennedy, B. J.; Shimakawa, Y.; *J. Solid State Chem.***2001**, *160*, 174.

DOI: 10.1006/jssc.2001.9216

40. Cullity, B. D.; Stock, S. R.; Elements of X-Ray Diffraction, 3rd Edition, Pearson Education International, p 170.
ISBN 10: 0201610914, **ISBN** 13: 9780201610918

41. Adamczyk, M.; Ujma, Z.; Pawełczyk, M.; *J Mater Sci.,* **2006**, *41*, 5317.
DOI: 10.1007/s10853-006-0300-8

42. Irvine, T. S.; Sinclair, D. C. West, A. R. *Adv. Mater.* **1990**, *2*, 132.
DOI: 10.1002/adma.19900020304

43. Kingery, W. D.; Browen, H. K.; Ulhman, D. R.; Introduction to Ceramics, John Wiley & Sons, New York, **1976,** pp 516.
Bookmark: http://trove.nla.gov.au/version/45656624

44. Mishra, R. K.; Choudhary, R. N. P.; Thakur, A. K.; *Journal of Alloys and Compounds,* **2008**, *457*, 490.
DOI: 10.1016/j.jallcom.2007.03.016

45. Mac Donald, J. R., *John Wiley & Sons,* **1987**, pp. 191-237.
ISBN: 0-471-64749-7

46. Moulson, A. J.; Herbert, J. M.; *Electroceramics, Chapman & Hall, London, U. K.,* **1990**.
ISBN 10: 0412473607, **ISBN** 13: 9780412473609

47. Dhak, P., Dhak, D.; Das, M.; Pramanik, K.; Pramanik, P.; *Mat. Sci. Eng. B.* **2009**, *164*, 165.
DOI: 10.1016/j.mseb.2009.09.011

48. Nobre, M. A. L.; Lanfredi, S.; *J. Phys. Chem. Solids,* **2003**, *64*, 2457.
DOI: 10.1016/j.jpcs.2003.08.007

49. Hirose, N.; West, A. R.; *J. Am. Ceram. Soc.* **1996**, *79*, 1633.
DOI: 10.1111/j.1151-2916.1996.tb08775.x

50. Jonscher, A. K. ; *Nature,* **1977**, *267*, 673.
DOI: 10.1038/267673a0

51. Almond, D. P.; Duncan, G. K.; West, A. R.; *Solid State Ion.* **1983**, *8*, 159.
DOI: 10.1016/0167-2738(83)90079-6

52. Funke, K.; *Prog. Solid State Chem.,* **1993**, *22*, 111.
DOI: 10.1016/0079-6786(93)90002-9

53. Elliott, S. R. ; *Philos. Mag., B,* **1978**, *37*, 553.
DOI: 10.1080/01418637808226448

54. Prasad, K.; Bagchi, S.; Amarnath, K.; Choudhury, S. N.; Yadav, K. L.; *Materails Science Poland.* **2010**, *28*, 317.